Instituto Superior de Engenharia de Lisboa

Área Departamental de Engenharia de Eletrónica e Telecomunicações e de Computadores

Platform for Photonic Sensor with Microfluidic

João de Vasconcelos Lopes Barroso
(Licenciado)

Dissertação de natureza científica para obtenção do grau de Mestre em Engenharia de Eletrónica e Telecomunicações

Orientadores:

Doutor João Costa
Doutor Miguel Fernandes

Júri:

Presidente:

Doutora Paula Maria Garcia Louro

Vogais:

Doutor João Costa
Doutor Alessandro Fantoni

Março 2024

Resumo

O presente documento visa o estudo e simulação de sensores fotónicos com base guias de onda de polímero fotossensível negativo com resoluções superiores a 1 μm e adaptáveis a sistemas de microfluídica.

A vantagem dos guias de polímero fotossensível negativo é evitar passos de fabrico mais complexos como a deposição por *plasma enhanced chemical vapor deposition* necessária quando se recorre, por exemplo, a guias de silício amorfo. Por outro lado ao direcionar o desenho dos sensores para resoluções superiores a 1 μm permitimos o uso da litografia de ultravioleta, evitando outras técnicas mais dispendiosas como a litografia por feixe de eletrões. Adicionalmente é de referir que os filmes de polímero são transparentes no visível permitindo o uso de fontes e detetores de luz a estes comprimentos de onda que são muito usados em biossensores.

Os resultados provenientes de simulação numérica mostram a viabilidade de um interferómetro com sistema de microfluídica com braços de comprimento de 9.3 mm, curva de saída de 90º com um raio de curvatura de 600 μm para um guia de onda com secção de 10 μm de largura por 4 μm de altura. Através de um estudo de otimização do alinhamento entre a fibra e o guia de entrada obteve-se uma atenuação menor do que 0.46 dB no acoplamento. A avaliação do impacto da altura dos canais de microfluídica revelou que para alturas superiores a 4.4 μm o desempenho do interferómetro não é perturbado pela dimensão do canal.

Key words: Interferometro, Biosensores, SU-8, Guias de onda de polimeros.

Abstract

This thesis aims to study and simulate photonic sensors based on negative photoresist waveguides with resolutions higher than 1 μm while being adaptable to mirofluidics systems.
Using waveguides made from negative photoresist polymers avoids complex fabrication processes such as the *plasma enhanced chemical vapor deposition* used on amorphous silicon waveguides. In addition to this by pivoting the design of the sensor into resolutions of upwards of 1 μm it enables the use of UV lithography which also prevents the use of more expensive lithography techniques. Additionally the polymer film is transparent to visible light making it possible to use light sources and detectors on the visible spectrum which are commonly used in biosensors.
The results from the numerical simulations shows the viability of making a interferometer with a microfluidic system with an arm length of 9.3 mm, a 90° degree exit curve and a 600 μm arc radius and with a waveguide with 10 μm width and 4μm height. Through the optimization of the alignment between the fiber and the waveguide an attenuation lower than 0.46 dB was obtained in the coupling. The evaluation of the impact of the height of the microfluidics channels showed that for height superior to 4.4μm the performance of the interferometer was not significantly disturbed.

Key words: Interferometer, Biosensors, SU-8, Polymer waveguides.

Contents

List of Figures

1
Introduction

1.1 Context and Motivation

There is a growing demand for biomedical devices that are portable and can provide diagnostic information in real time. The traditional approach of having samples taken from a patient and sent to the laboratory is not time-efficient and has considerable costs associated. In 2020 we have seen the importance that test kits had in the management of the COVID-19 epidemic. More recently the kits have been upgraded with screening additional virus, such as influenza virus type A and others. We are in the path of producing real lab-on-chip devices that can screen for multiple diseases.

In order for such devices to have an impact on society they need to be portable and inexpensive. One possible approach is the use of photonic refractive index sensors. In a photonic refractive index sensor the surface is made sensitive to the analyte that should be detected. When the analyte contacts the surface of the waveguide the effective refractive index changes and this causes a change in some measurable light property, such as intensity or a phase-shift.

A promising approach is the use of interferometers which are very sensitive to refractive index changes. Nevertheless the production of such devices usually relies on expensive fabrication methods, namely electron beam lithography and deposition of films with very specialized equipment.

In addition throughout the last decade negative photoresist polymers, such as SU-8, have been explored as photonic waveguides with the advantage of being easily made by spin coating and being transparent to visible light. This could help decrease the cost of the sensor production.

1.2 Objectives

The aim is to study the feasibility of a photonic interferometric sensor based on waveguides of a negative photoresist polymer (SU-8) with the added feature of being adaptable for a microfluidic system. The goals will be divided into different tasks:

• Determining the length of the arms of the interferometer having in consideration the choice of materials and the requirements in terms of minimum feature size of the waveguides;

• Determining the minimum curvature radius of the waveguide for an attenuation of less than 0.5dB;

• Determining the input coupling between a multimode fiber and the input waveguide

• Study the impact of the microfluidic channel on the performance of the interferometer.

The minimum feature size of the waveguides mentioned in the first task was defined based on the typical range of thickness indicated for SU-8 applications and the width of the waveguide that makes the device capable of being made through UV lithography. With this in mind the minimum feature size of the waveguides was made to be 10 μm wide and 4μm thick.

1.3 Organization of the Document

This thesis consists of several chapters which will be described in this section. In the first chapter is given an introduction the objectives placed on this project.

The second chapter provides an overview of the state-of-the-art with relevant literature and the works that served as the basis for this thesis.

The third chapter focus is on giving an insight into the methods that were used in this work, these include both the methods required for the numerical simulations as well as the ones required for the fabrication of the device. Even though the sensor was ultimately not fabricated it was decided to include the fabrication methods since they would have an impact in the definition of the design requirements for the simulation with the added benefit of leaving room to explore the fabrication in future work.

A fourth chapter contains the proposed design supported with the results obtained during the numerical simulations while explaining the reasoning behind the choices made.

The fifth and final chapter is devoted to the discussion of the results as well as the conclusions and the future work that can be explored.

2
Fundamentals and State of the Art

Over recent years the need for portable, rapid and inexpensive devices for biosensing has become greater. While conventional methods of detection provide high performance and significant specificity, their process is normally performed with the use of bulky and expensive instruments while also being lengthy, time wise. This justifies the efforts put into the development of portable, highly integrated and cost-effective devices that can perform such tasks.

With the use of small compact biosensors or Lab-on-Chip devices we can identify and measure the chemical constituents of the substances we wish to study through the monitoring of their optical properties such as absorption, fluorescence, chemiluminescence or their refractive index. Through the use of these devices we can achieve a quick response time and high performance in terms of sensitivity and reliability. In most cases these devices work by recognizing changes in the refractive index of the biological sample and relating it to the concentration of the analyte in question. Such a method doesn't require hazardous chemicals, and is done in a way that does not destroy the analyte, avoiding the need to use a substantial volume of samples.[16]

2.1 Microfluidics

Microfluidics is an emerging technology that consist in the manipulation of small volumes of fluids, typically in the nano to pico litters. This can be accomplished by the use of microchannels with dimensions of micrometers or even smaller. This field has evolved over the past years to encompass a wide range of applications, which can include fluid mixing, pumping liquids, cell culturing, and others. Due to the small dimensions of the microchannels, the fluidic system has a low Reynolds number that makes the controlled laminar flow systems easily achieved.

Microfluidic devices have the advantage of being small and thus portable. These devices also have an inexpensive platform for rapid prototyping that makes the fabrication cost and time being significantly reduced, showing the possibility for mass production. There have been numerous efforts to integrate microfluidics into other areas, such as electronics, optics and acoustics. Recently photonics has been integrated into microfluidic chips making a new field referred to as *optofluidics*, where microfluidic photonic integrated circuits are included [17].

In the case of *optofluidics*, there is a growing interest in refractometry-based sensors for flow analysis, since they have simple structures, high sensitivity and benefit from label-free detection. These sensors can measure tiny changes in the refractive index on the sensing region, with its architecture illustrated by the figure 2.1, which makes it appealing for monitoring molecular interactions and chemical reactions with applications on numerous fields including biomedical detection, chemical analysis and food safety [18].

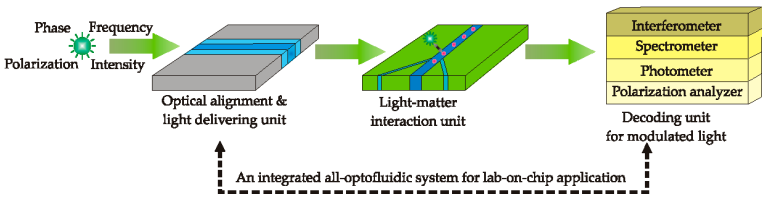

Figure 2.1: Ideal optofluidic system for lab-on-chip (adapted from[1])

2.1.1 SU-8

Polymer-based integrated photonics offers many advantages over silicon materials. For the purpose of integrated optics, polymers have been used to improve electro-optical and optical non-linear effects. Even though polymers usually have lower tolerance to high temperatures, that are commonly used in the fabrication processes, if these high temperatures can be avoided the polymer can represent a lower cost of fabrication, which can be desirable especially in disposable devices like in the case of optical/biosensors. In the case of biosensors the polymer based sensor confers even more advantages such as the fabrication flexibility, reliability, low power consumption and potential for mass production while having a lower cost of production.[19]

Although there are a number of choices for optically transparent polymers for fabrication of photonic structures, one that has gain traction is the SU-8 polymer. This material has a high mechanical stability, and a low cost.[19] SU-8 is a high aspect ratio negative photoresist used for its properties. It has a wide range of coating thickness where the deposition layers can range from several hundreds of nanometres to several hundreds of microns for a single

spin coating step, with this being easily controlled by adjusting the spin speed and the its viscosity as stated by the manufacturers.

The SU-8 polymer is an epoxy-based photosensitive polymer that is very versatile. It has a low electrical conductivity and a very high optical transparency in the visible and infra-red region of the electromagnetic spectrum (region where the laser that is to be used will operate). Moreover as shown in the figure 2.2 this polymer as a low absorbance and a low extinction coefficient beyond the 400 nm wavelength.[2]

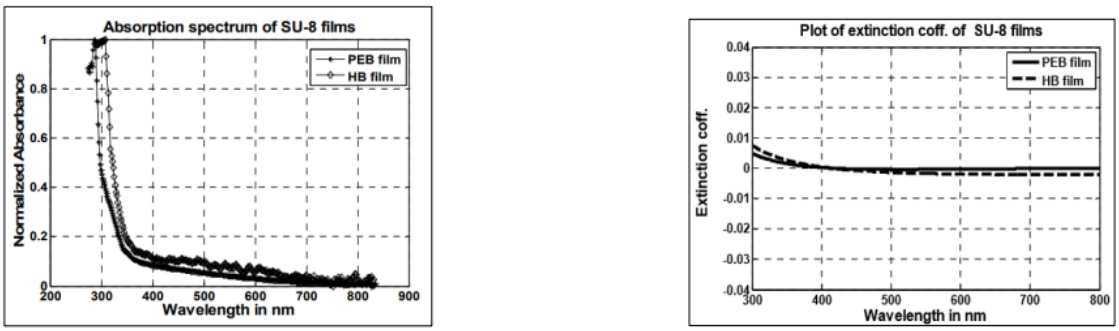

Figure 2.2: Absorption Spectrum and Extinction Coefficient of SU-8 films (adapted from[2])

This material also displays a refractive index in the 1.57 to 1.58 range for the operating point of the laser (635 nm), which can be seen in the figure2.3.

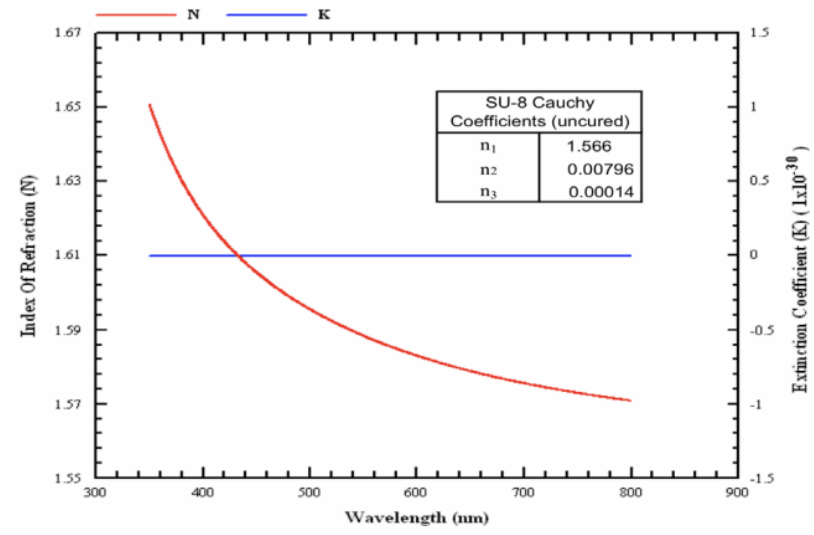

Figure 2.3: SU-8 Cauchy coefficients (adapted from [3])

Adding to this the SU-8 polymer can be modified in order to accommodate specific biomedical applications, namely immobilizing biomolecules for biosensing. This makes this polymer optimal for biomedical applications.

Due to its proprieties SU-8 is also a good material for the fabrication of microchannels since it has an excellent chemical stability against acids and

bases as well as the great thermal stability. For these reasons this material has a wide range of applications in microfluidics [20]. This would confer the sensor the ability to be adapted into a microfluidics system or having a microfluidics system integrated onto it.

While these sensors can operate with different detection methods the one that is going to be focused on is the refractive index detection method. As a consequence of the biomolecular reactions happening in the waveguide surface the result is a change the effective refractive index which can be measured and monitored through the intensity at the end of the waveguide. The sensor to be designed in this thesis will work based on this method of detection as a mach-zehnder interferometer.

There are advantages of using an evanescent field based detection as it is non-damaging and enables real-time, multi-analyte monitoring.[21]

The following figure 2.4 shows a standard process of handling SU-8 as stated in the data-sheet of the material.

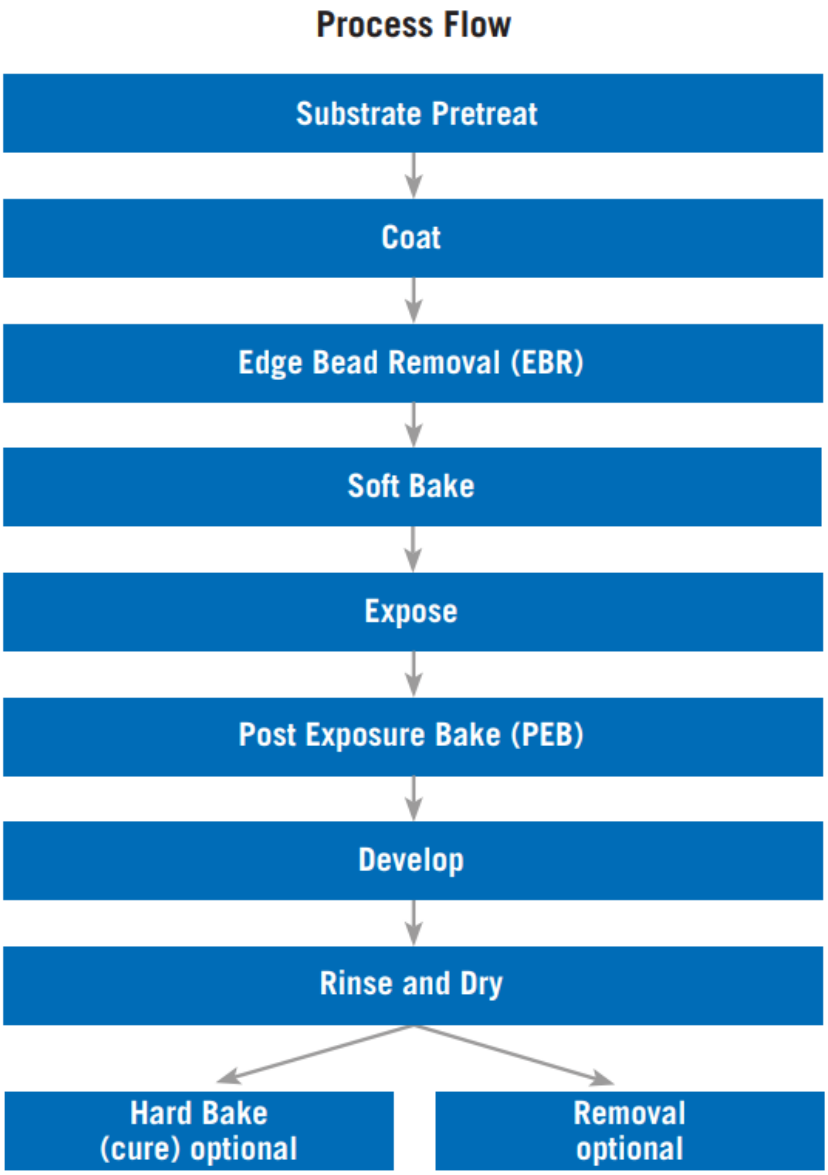

Figure 2.4: Common Process of handling SU-8 (adapted from [3])

2.1.2 Mach-Zehnder Interferometer

A Mach-Zehnder interferometer is a device that relies on the interference of the waves, both constructive and destructive. The interferometer is used to determine the relative phase shift between two collimated beams from the same source.

These interferometers have yielded excellent detection limits. They are particularly sought after due to their design freedom which allows for applications in point-of-care compatible read-out schemes.[10]

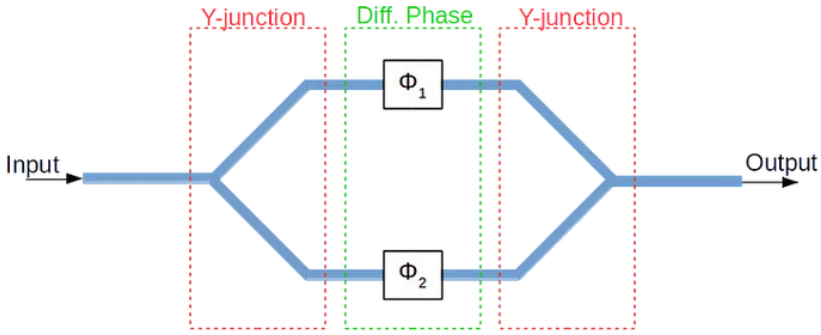

Figure 2.5: Mach-Zehnder Interferometer representation (adapted from [4])

In the figure 2.5 a representation of a Mach-Zehnder Interferometer device is shown. The beam splitting and merging for the two channels is done by two Y-junctions. The interaction zone at the sensing interferometer channel is formed by allowing the medium under analysis (analyte) to influence the evanescent electromagnetic field. This interaction results in a modification of the phase and intensity of the light present in the channel. Once the beam reaches the merging section the intensity of the light is modulated due to the interference.[22] The interference can be destructive or constructive depending on the accumulated phase difference. As such, the accumulation of phase is translated into a change in the transmitted amplitude which varies as a function of wavelength.[10]

Integrated optical Mach-Zehnder interferometer pose distinct advantages over other optical transducers such as being able to increase the sensitivity by increasing the interaction length and also having a reduced thermal and mechanical noise which greatly improves the detection limit of the biosensor.[23]

2.2 Methods used in Sensor Production

In the manufacturing process of the sensor some techniques are used. In this section some methods, which are commonly used in the fabrication of the photosensor are going to be described. The methods were chosen based on the materials that were considered for this work as well as the equipment that was available at the time.

2.2.1 Spin Coating

Spin coating is a common technique in order to apply thin films onto substrates. This is achieved by spinning the solvent and the material at a high speed so that the centripetal force and the surface tension of the liquid create an even covering of the material.

Spin coating usually is done by applying an a thin film which can be from anywhere between a few nm to a few μm evenly across the surface of the substrate by coating a solution of the desired material in a solvent while it is rotating. The rotation of the substrate is usually higher than 10 rotations per second or 600 rpm.

The process of spin coating can be divided into 4 main steps (as shown in the figure 2.6):

- Deposition
- Spin up
- Spin off
- Evaporation

In the first step the solution is deposited onto the substrate. This deposition can be done before the substrate is spinning(Static spin coating) or while it is already spinning(dynamic spin coating).

After a lower-speed spreading step the substrate reaches the desired rotation speed. In this stage most of the solution is expelled from the substrate.

Afterwards the fluid begins to thin and will start to dry.

The spin coating technique has some advantages such has its simplicity and ease with which the process can be set up while the high spin speed makes it so that the drying time is reduced and this results in a higher consistency at macroscopic and nano length scales. This is also coupled with the fact that spin coating is relatively cheap.

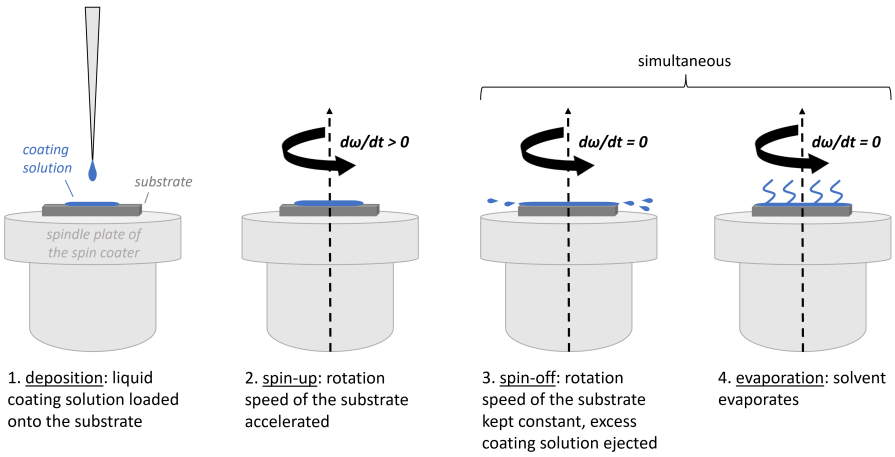

Figure 2.6: Spin coating steps (adapted from [5])

2.2.2 UV Lithography

Photolithography is a process that is commonly used to manufacture integrated circuits. This is done by transferring a pattern onto a substrate using electromagnetic radiation, which is commonly UV light. The photolithogra-

phy process begins with a photosensitive material, named photoresist, being applied to the substrate. A photomask containing the pattern that is to be etched onto the circuit is then placed over the photoresist. The photomask is then shone with electromagnetic radiation exposing the photorisist in certain areas, due to the fact that the exposure to the radiation modifies the solubility as a result of chemical changes in its structure. This is then followed by the developing of the material. The photoresist is immersed in solvents which will dissolve either the exposed region (in a positive photoresist) or the unexposed region (in a negative photoresist). Finally the pattern transfer is done through an etching process.[24]

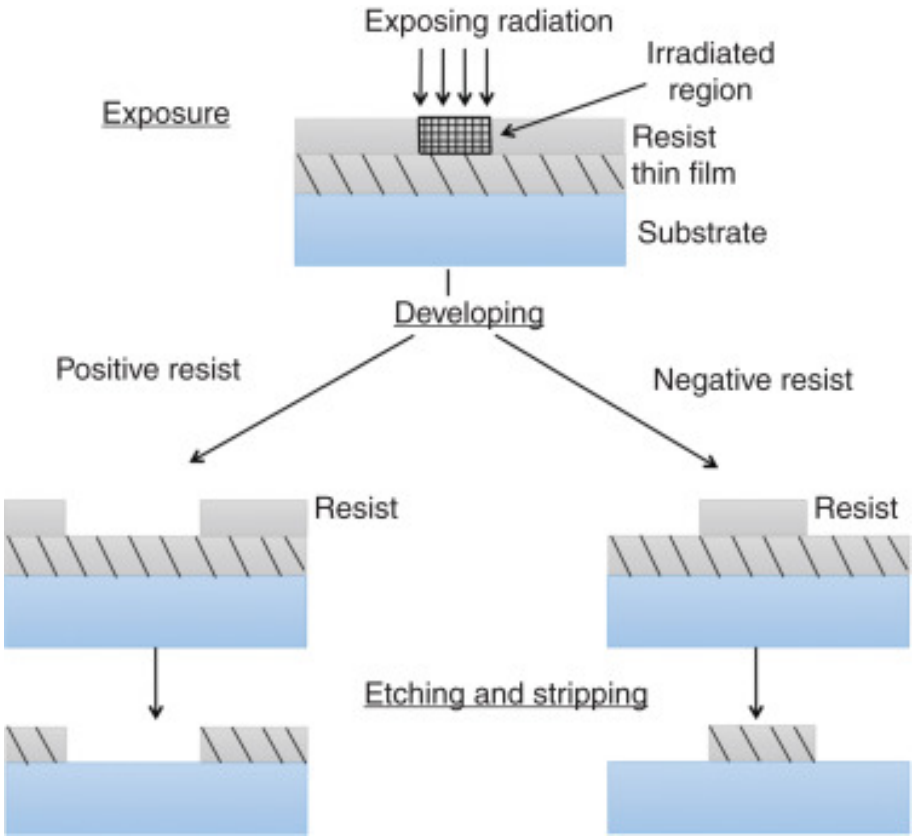

Figure 2.7: UV Lithography method (adapted from [6])

2.2.3 Optical Sensors

Integrated optical sensors have engrossed specialists of the field for the past two decades. The operation of such optical sensors does not interfere with the external electric or magnetic fields and they are more accurate than their electrical counterparts.

There are two major categories of integrated optical sensors: absorptive and interferometric with the interferometric being preferred due to their function not being dependent on the absorption of the analyte which in some instances can be low in the visible to near infrared regions.[25]

There has been an effort in order to study the feasibility of photosensors using different materials and with different configurations. Here some of the works done in order to study photonic sensors in particular those based on Mach-Zehnder interferometers are presented as to give some context of what has been done in this field as well as to show some applications and results these studies have yielded.

2.2.4 Relevant Previous Work

On-Glass Integrated SU-8 Waveguide and Amorphous Silicon Photosensor for On-Chip Detection of Biomolecules: Feasibility Study on Hemoglobin Sensing

One such sensor is the one studied in the article "On-Glass Integrated SU-8 Waveguide and Amorphous Silicon Photosensor for On-Chip Detection of Biomolecules: Feasibility Study on Hemoglobin Sensing" by Alessio Buzzin.[7] In it the objective was to make an inexpensive and easy to use Lab-on-Chip that can evaluate biological analytes. This sensor would work through refractive index detection. This means that the sensor would detect the variation in the optical properties mainly the refractive index and the extinction coefficient in respects to the concentrations of the analyte that is deposited in the interaction site which is depicted in the figure 2.8.

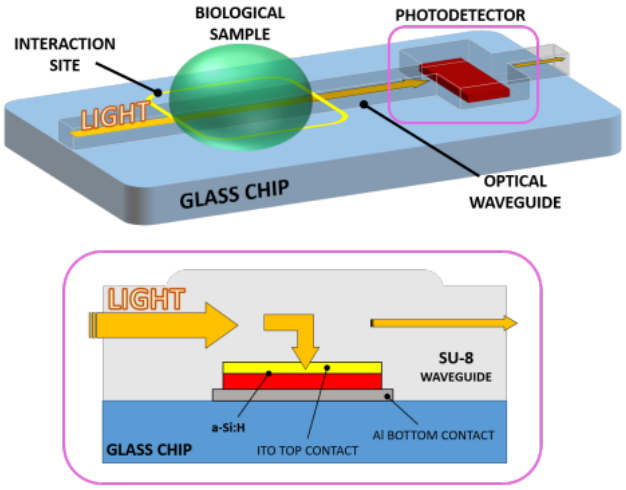

Figure 2.8: Sketch of the photosensor for on chip detection of biomolecules (adapted from[7])

In this study the results indicated that the limit of detection for hemoglobin could reach 100ppm which is in line with the colorimetric methods that are currently on the market with the prospect of improving upon the design by changing the waveguide thickness and the interaction site length.

SU-8 waveguiding interferometric micro-sensor for gage pressure measurement

Another instance of a on-chip Mach-Zehnder interferometer is the one seen in the article titled: ”SU-8 waveguiding interferometric micro-sensor for gage pressure measurement” by N. Pelletier.[8] This work studies the modeling and realisation of a micro-sensor based on a convenient optical principle, a Mach-Zehnder interferometer based on SU-8, depicted in the figure 2.9. The sensor would be used to gauge pressure by measuring disturbances due to optical path variations.[8]

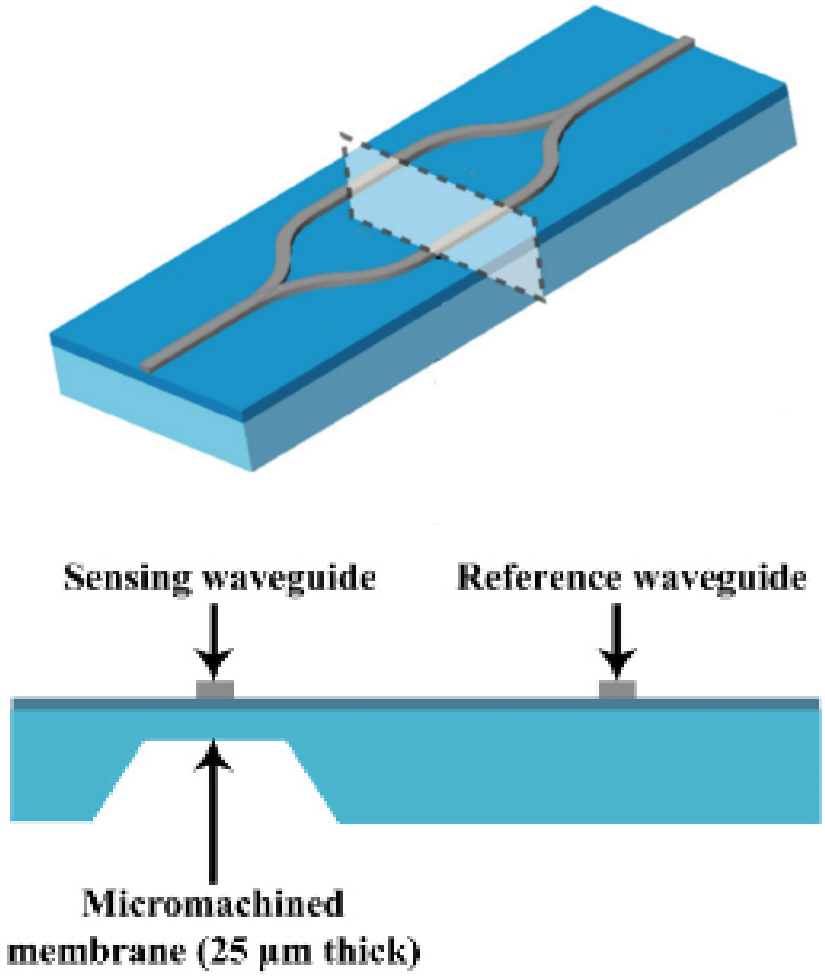

Figure 2.9: Sketch of the Mach-Zehnder Interferometer (adapted from[8])

This study yielded a proper gauge measurement range in the 2×10^5 Pa above atmospheric pressure. The actual realized interferometer is represented in the figure 2.10.

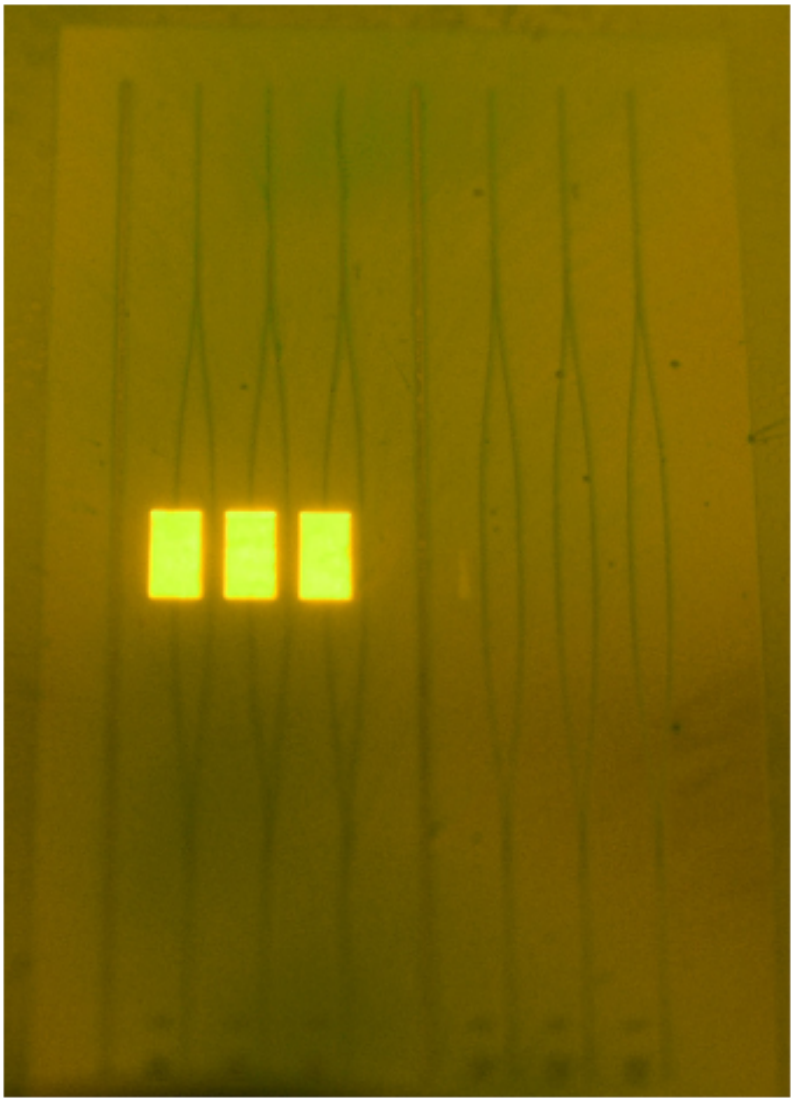

Figure 2.10: Realisition of the Mach-Zehnder Interferometer (adapted from[8])

SU-8 micro-biosensor based on Mach-Zehnder interferometer

Other papers dealt with the same problem such as the one titled ”SU-8 micro-biosensor based on Mach-Zehnder interferometer” where an optical biosensor made using a Mach-Zehnder interferometer as the base configuration is designed and simulated. As stated before this type of sensor can offer an array of advantages such as compactness, real-time analysis, low cost, high sensitivity and the possibility of integration of electronic detection components on the same chip.[9]

This work focus on the simulation aspect of the design. In this work the simulation of a biosensor that consists of a SU-8 polymer strip optical waveguide integrated on a silicon substrate with an immobilized bio-sample on top of the core of the waveguide (represented on the figure 2.11) showed that the

output of the signal was able to be detected and analyzed with an integrated photodiode. It also showed that the effective refractive index was strongly dependent on the light polarization which showed different responses to the TE and TM waves.[9]

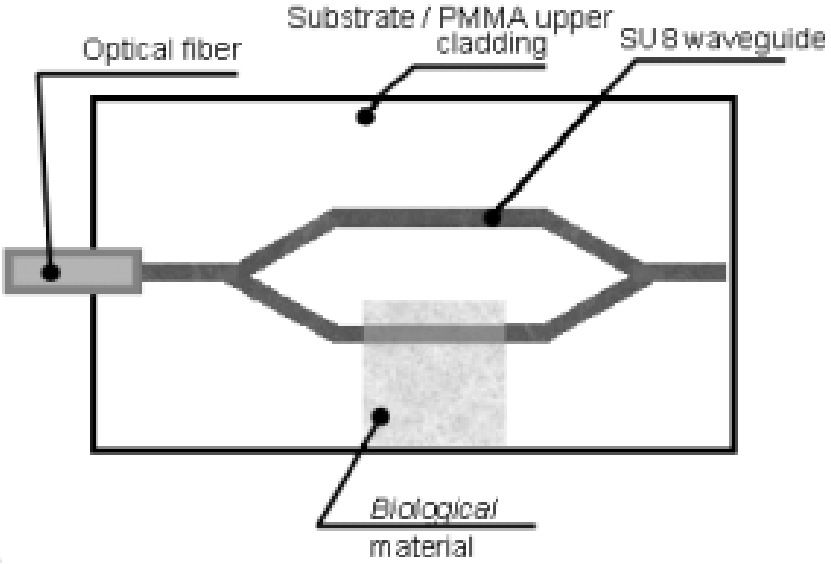

Figure 2.11: Mach-Zehnder Interferometer biosensor from Psoma's work (adapted from [9])

Modeling and simulation of opto-fluidic based Mach-Zehnder interferometer for biosensing application

In the article done in 2017 and with the importance of a rapid diagnostic test for dengue surveillance in the effectiveness of the disease surveillance, the use of an integrated optical Mach-Zehnder interferometer was studied. This biosensor was designed to realize the surveillance throught platelets count.

A Mach-Zehnder interferometer with a liquid core waveguide in the sensor arm for the surveillance of dengue was studied. In this paper the interferometer was successfully simulated using a single mode fiber working at the 1550 nm wavelength.[23]

Study on the limit of detection in MZI-based biosensor systems

In the work by Martens the limit of detection and the effects of some types of noises was studied. This provides a blueprint of optimization of a Mach-Zehnder interferometer sensor, having the one on the figure 2.12 as reference, under any combination of read-out method and measurement circumstances.

This was backed by a set of experimental results that comfirm the validity of the theoretical results.[10]

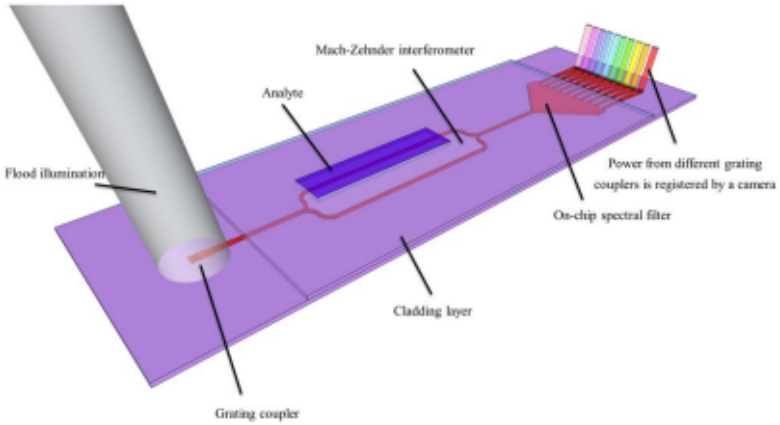

Figure 2.12: Mach-Zehnder Interferometer biosensor from Martens's paper (adapted from [10])

3
Methods and Materials

3.1 Simulation Methods

Optical simulation tools are a powerful complement to microscopy and theory in order to provide an explanation of the observed optical effects. While analytical theory can be used to explain the more simple structures, the more complex structures that are common in biology require more sophisticated numerical simulation where the numerical approximations to the physical equations are solved iteratively until they converge into a solution. These simulations methods can vary depending on the variables at play.[26]

For the purpose of designing a sensor a simulation phase as to be done this requires a software that can simulate the optical and photonic devices in order to better gauge the viability of the proposed sensor.

In this section it will be discussed the software used as well as its main methods of simulation.

3.1.1 RSOFT

In order to design and optimize the sensor the RSOFT software was used as it enables the design and simulation of optical telecommunication devices, optical components and photonic devices. The software's main feature is the CAD environment, exemplified in figure 3.1, that allows to create systems for design of waveguide devices and other photonic devices. It also serves as a control program for the passive device modules which includes the BeamPROP, FullWAVE, BandSOLVE, GratingMOD, DiffractMOD, FemSIM and ModePROP and defines the material properties and the structural geometry of the devices.

Through the use of RSOFT it was possible to optimize the parameters of the sensor such as the waveguide and substrate dimensions.

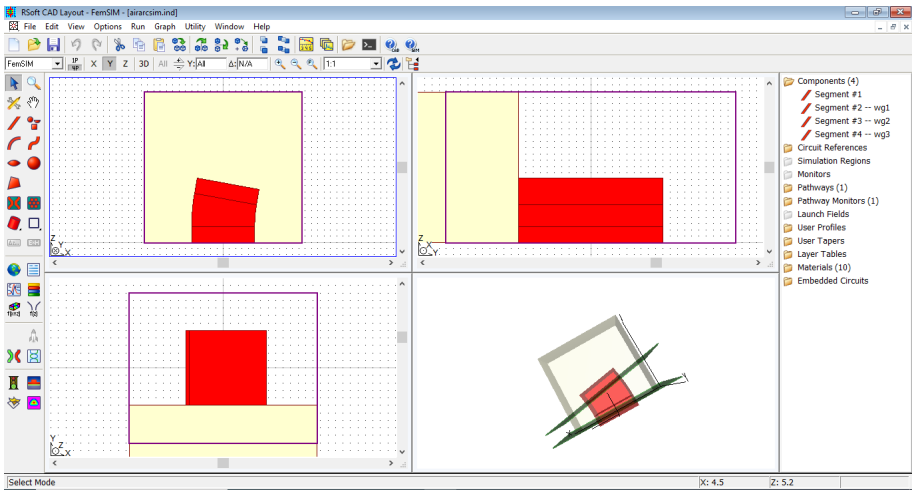

Figure 3.1: RSOFT CAD environment

This software uses various types of method of simulations such as:

- Finite Difference Time Domain Method;
- BeamProgation Method;
- Finite Element Method.

Finite Difference Time Domain Method

The Finite-difference Time-domain method (FDTD), also called Yee's method after the inventor of the method, is a numerical analysis technique that is used for modeling computational electrodynamics, meaning that it finds the approximate solution to the associated system of differential equations. Being a time-domain method it covers a wide frequency range with a single simulation. The FDTD can be applied to calculate reflectance, transmission, diffraction, interference, and absorption of different materials.

This method solves Maxwell's equations on a mesh and computes the E and H grid points spaced Δx, Δy, and Δz apart, with E and H interlaced in all three spatial dimensions. Simulations using the FDTD method can account for scattering effects, transmission, reflection, absorption, etc. As stated before this is a time-domain method but with the use of the FFT (Fast Fourier Transform) and the DFT (Discrete Fourier Transform) it is possible to have a frequency analysis.

While FDTD was first introduced in 1966 more efficient features and algorithms have been developed over the past five decades, including parameter sweeps over many features of interest. Now FDTD is a widely-implemented method of simulation which is available in well-documented commercial and open-source programs. FDTD simulations are particularly well suited for broadband simulations, meaning simulations in which light sources contain a large wavelength range, as well as for determining the behavior of light over time,

from when it is emitted from the source through its interaction with the object and beyond.

In a more practical scenario this method of simulation has been used in to help researchers understand experimental data as well as evaluating hypothesis regarding the nature of structural color and other optical effects at the micro and nano-scale as stated in the paper by Dakota E. McCoy [26].

In the RSOFT software this simulation method is used in the FullWAVE simulation where it performs a full-vector simulation of photonic structures. It is a highly sophisticated tool in order to study the propagation of light in a multitude of photonic structures such as waveguides, this being the focus in this work.

This technique comes with a high demand on the processing capability, meaning that lower end machines will require a great amount of time in order to complete one simulation.

Beam Propagation Method

The beam propagation method (BPM) is one of the most widely used for studying the light propagation in longitudinally varying optical waveguides. Adding to this there are a great number of versions of the beam propagation method such as the beam propagation method based on the fast Fourier transform, the Beam Propagation Method based on the finite difference method and the one based on the finite element method.[27]

The beam propagation method is an approximation technique for simulating the propagation of light in various waveguides. This is a quick and easy method of solving for fields in integrated optical devices. It is usually used to solve for intensity and modes within a shaped waveguide structure.

This method usually reduces the problem to a one-dimensional cross-sectional index profile by defining effective indexes to various parts of the structure, then it solves the paraxial wave equations for the resulting profiles[28]. This makes it so that the technique can be inadequate for certain cases. In layman's terms the beam propagation method decomposes a mode into a superposition of plane waves traveling in different directions. These individual waves are propagated through a finite predetermined distance through the waveguide until the point where the field needs to be determined. At this point, all the individual plane waves are numerically added in order to get back the spatial mode.[29]

In a more practical sense the beam propagation can be used in simulations on various photonic crystals circuit components and optical gratings with modulated refractive indexes as shown in the paper by Koshiba M [30]. Another example of the use of this method is the one described in the paper

cited previously by Tsujil [27], where it is shown the validity of the simulation results from the method for Gaussian-beam excitation of a straight rib waveguide.

In the RSOFT software this method is used as a low resource and fast simulation tool used to extract the effective refractive index throughout the waveguide in order to calculate the dimensions of the sensor.

Finite Element Method

From a theoretical perspective the development of numerical methods to solve the Maxwell's equations of an Electromagnetic wave is an important venue of research as the prediction of the Maxwell's equations gives an excellent description of the phenomenology of these exhibited by the systems in study.

This method allows one to study geometries of arbitrary complexity, it can deal with frequency dependent dielectric functions in a natural way, discontinuities in the dielectric function are not especially detrimental for convergence of the method, and the quantities are already calculated in the stationary regime.[31]

The Finite Element Method (FEM) is a numerical method for solving differential equations. In order to solve the problem the FEM subdivides a large system into smaller, simpler parts called finite elements. With the behaviour of each element determined, they can then be patched together which enables an approximate solution of the entire body over the entire domain.

In the paper cited above the finite element method is used in order to demonstrate the its stability, robustness and reliability in the study of the light propagation and confinement in both periodic and aperiodic dielectric photonic crystals.[31]

This method is used in the RSOFT software in order to determine the modes of propagation and their characteristics, while also determining the effective propagation constant of the desired section.

3.2 Photomask Design Software

For the purpose of designing the photomask the *KiCad* software was used as it allows for the rigorous design of the mask while also allowing the export of the data file (Gerber file) that is needed for the realization of the actual mask.

3.2.1 KiCad

KiCad is a software suite for eletronic design automation. The software facilitates the design and simulation of electronic hardware for PCB manufacturing. It has an environment for schematic capture and PCB layout, manufacturing file viewing. Within KiCad there are tools to create bill of materials, artwork, gerber files, and 3D models of PCB and its components. A representation of the KiCad environment is presented in the figure 3.2

As stated before the KiCad software was chosen since it has the ability to produce a Gerber file that is required for the realization of the photomask.

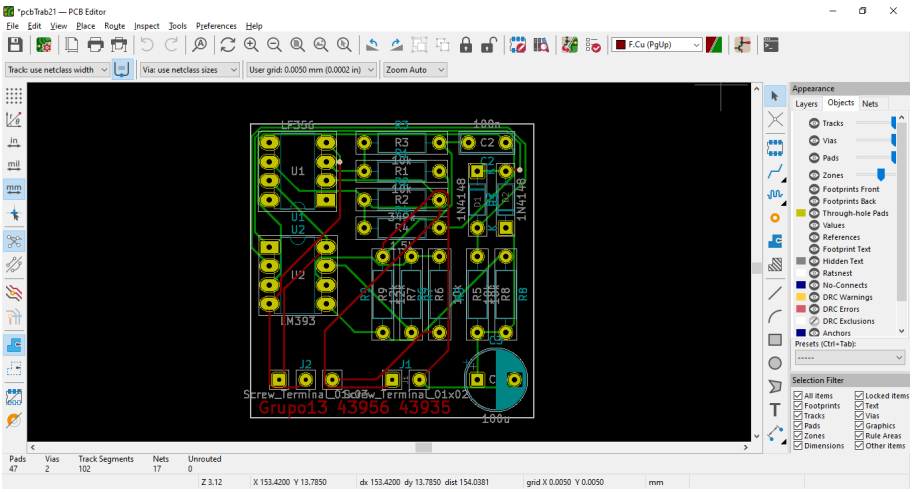

Figure 3.2: KiCad Environment

3.2.2 Mask

One of the approaches for the lithography is the use of a photomask which is an opaque plate that has some transparent areas in order to allow the light to pass through in a certain pattern. As stated in the previous section this mask is used in the photolitography in order to project a pattern in the photoresist.

This can also be done by direct laser writing which is a technique capable of altering the chemistry of the material over different surfaces following a layout or pattern, as ilustrated in the figure 3.3. These patterns can be achieved with processes such as ink jet printing, dip pen nano-lithography, and micropens to add material to the substrate based on a CAD layout.

In this work the idea was to use direct laser writing using the KiCad to design a ”mask” in order to write the pattern onto the waveguide.

Through the use of the KiCad a computerized data file is created which is then converted into ”coordinates” that in turn are written into the plate. This is were the KiCad is used as it produces the data file used to produce the mask.

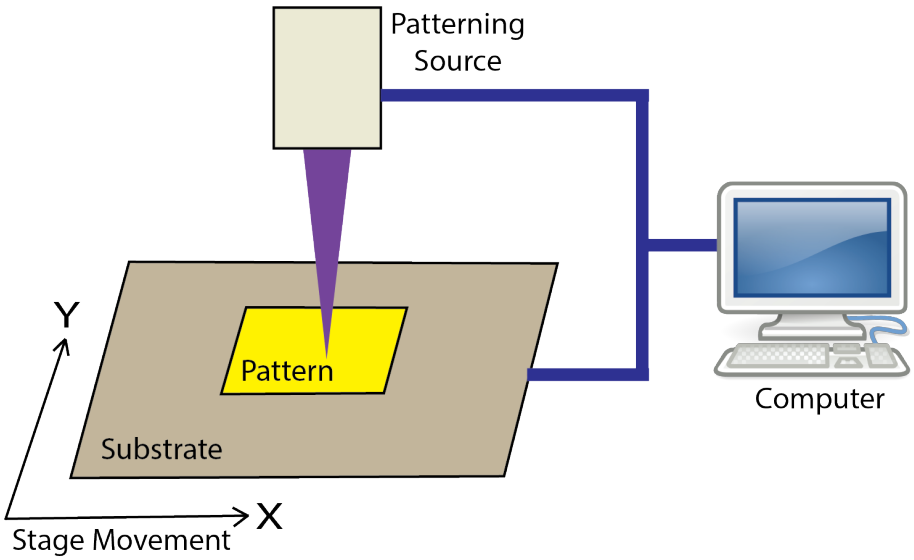

Figure 3.3: Direct Laser Writing (adapted from [11])

4
Results and Discussions

In this section the work done as far as simulations and prototypes of the sensor will be discussed.

The sensor is based on a Mach-Zehnder interferometer. By doing so it will allow us to measure the relative phase-shift variation between two beams derived from the same source by splitting the light in a Y-junction. This phase-shift will be translated into a change in the transmitted amplitude.

The figure4.1 shows a representation of the sensor.

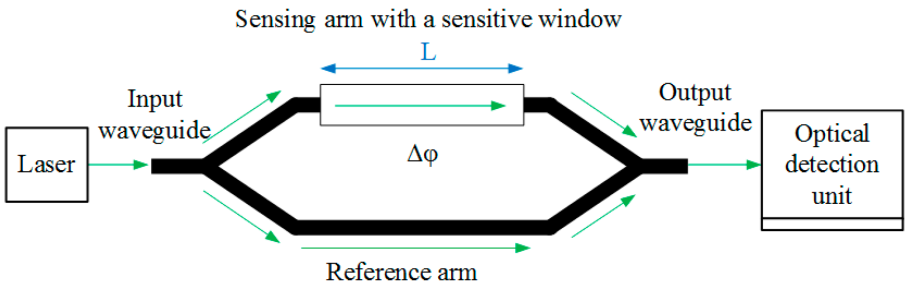

Figure 4.1: Sensor representation (adapted from [12])

Most of the work done was made through simulations using the RSOFT sorftware which allows the simulations of optical components.

In order to start the simulations a model of the sensor was made in RSOFT. Because of the large dimensions of the sensor a complete simulation of the interferometer using FDTD is not possible with the available computational resources. A few simplifications were introduced in particular each arm of the interferometer was studied separately. In the figure 4.2 the region that is going to be modeled and simulated in the software is highlighted in yellow.

Figure 4.2: Region of the sensor to be modeled and simulated

Taking into consideration the works which had a similar sensor as the one in this thesis, as well as the limitations of the production derived from both the equipment and the techniques available, the substrate model was assumed to have a width of 12 μm shown in the figure 4.3 with the W_{sub} label and a height of 2 μm labeled in the figure by h_{sub}.The material used as the substrate was corning glass with a refractive index of 1.5053. As it was done with the substrate the dimensions of the waveguide were also assumed based on the previous factors. This resulted in the waveguide having a width of 10 μm labeled as *W* and a height of 4 μm labeled *h* while having the optical proprieties of the SU-8 material mentioned in the SU-8 section of this thesis.

The sensor in this work was designed to work with water as its sensing medium since this would facilitate the experimental tests. As a consequence to this the design of the sensor was optimized for maximum variation of output power in the presence of water in the sensing arm.

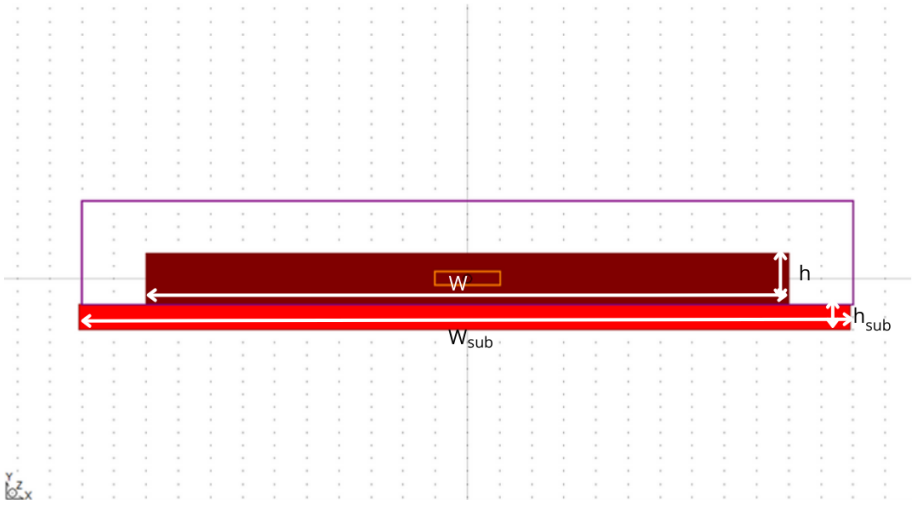

Figure 4.3: Frontal View of the Sensor Model
Color label : Dark Red - SU-8 Waveguide
Light Red - Corning Glass Substrate

4.1 Modes of Propagation

An important part to the study of the sensor is determining what modes propagate through the waveguide and selecting the mode which will be used in this thesis.

The modes of propagation in a waveguide are divided into two categories: *Transverse Electric Mode* and *Transverse Magnetic Mode*. In the first mode the electrical field vectors are transverse to the direction of propagation which means that there is no electrical field component along the direction of propagation. In the second mode similarly to the first a component of the electromagnetic wave is perpendicular to the direction of propagation, with this component being the magnetic field.

In order to ascertain the modes of propagation that will be traveling along the waveguide there was the need to use the FEMSim tool of the RSOFT software. This will give the modes of propagation as well as the propagation constant of those modes.

The results of the simulations are presented below where it's possible to see that the components E_y (figure 4.4), H_x (figure 4.5) of the TM fundamental mode are being propagated, almost entirely, through the waveguide, as well as the components E_x (figure 4.6) and H_y (figure 4.7) of the TE fundamental mode.

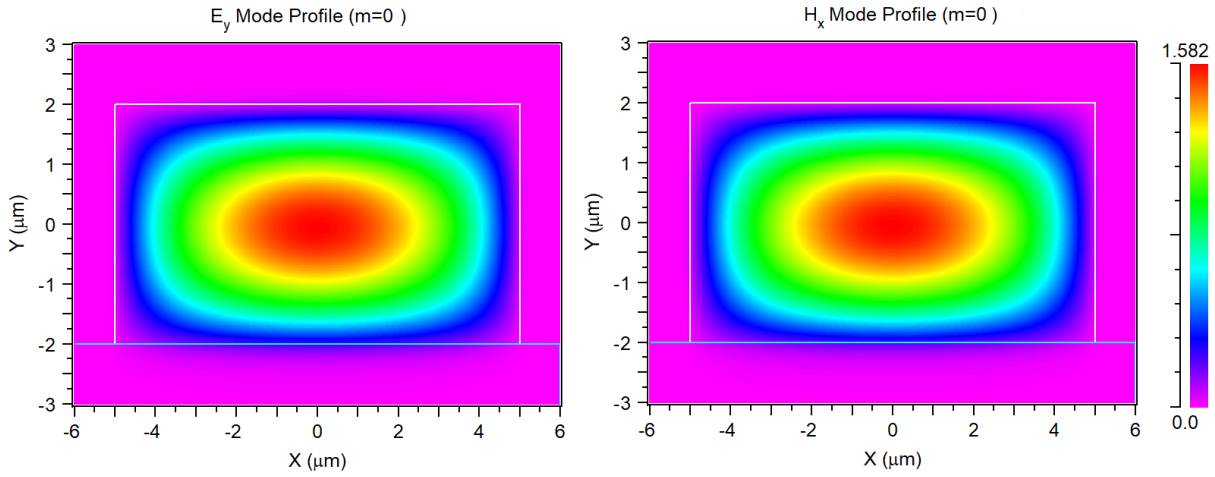

Figure 4.4: E_y Component of Fundamental mode TM

Figure 4.5: H_x Component of Fundamental mode TM

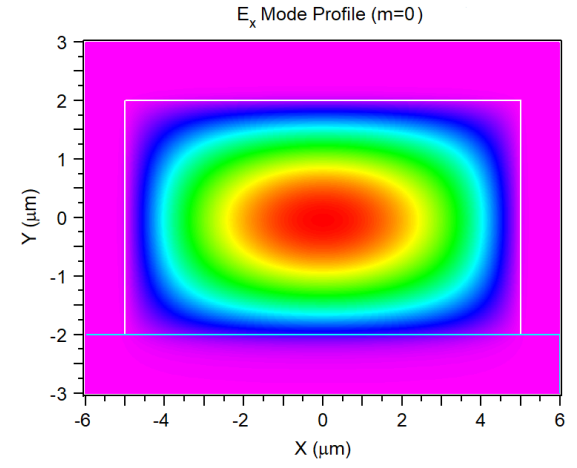

Figure 4.6: E_x Component of Fundamental mode TE

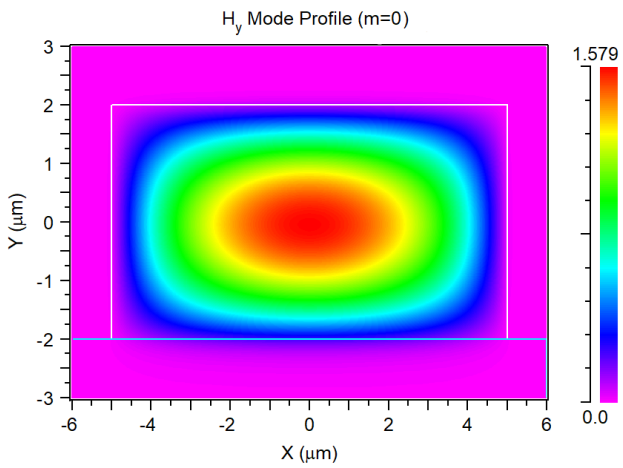

Figure 4.7: H_y Component of Fundamental mode TE

For the sake of this work the mode that is going be focused on is the fundamental TM mode. The TM fundamental mode was chosen as the ”single mode” since it will be assumed that only one mode is going to be propagating in the waveguide as this would limit the interference between modes. Another reason for this choice is the fact that the TM mode has a higher tendency to leak out of the waveguide in the vertical direction. This makes it more sensitive to the surrounding medium.

4.2 Sensor Dimensions

One of the limitations of the sensor production is the dimensions of the sensor itself. In order to calculate the length of the sensor mainly its arms the following equation is needed as it provides a way to calculate the length of the arms of a Mach-Zehnder interferometer (d):

$$d = \frac{1}{\frac{n_{eff_2} - n_{eff_1}}{\Delta\phi} * \left(\frac{2\pi}{\lambda}\right)} \tag{4.1}$$

In the equation 4.1 the n_{eff} is the effective refractive index, which is the variable that quantifies the phase delay per unit length in a waveguide relative to the phase delay of the vacuum. The parameter n_{eff_2} is the effective refractive index of the waveguide when in contact with the analyte (the sensing arm) and the n_{eff_1} is the effective refractive index of the waveguide when it's in contact with the air (reference arm). Both values of the effective refractive index will be acquired through simulation. The $\Delta\phi$ is the phaseshift between both arms, which will be π since this would translate in an output amplitude of 0 which would be a result of recombining the same wave in phase opposition. Lastly the λ is the wavelength at which the laser will be operating in.

This value was chosen to be 635 nm as this is a common operating point of red light lasers as well as being the operating point of the lasers that were available in the lab.

Using the FEMsim tool in the RSOFT software the model previously described was simulated in order to chose the height of the waveguide as well as calculate the dimensions of the arms of the sensor. These simulations had the goal of finding both effective refractive indexes of both arms of the sensor, the sensing and the reference arm, and also calculating their length in relation to the height of the waveguide.

For this purpose a set of simulations were performed where the height of the waveguide was changed from 1 μm to 5 μm, in increments of 0.5 μm. Coupled with this the background material was also changed from air to water in order to get both the n_{eff} for the reference arm and the sensing arm respectively.

The figure 4.8 and the figure 4.9 were generated from the simulations where it is shown the evolution of the effective refractive index of the waveguide with its height.

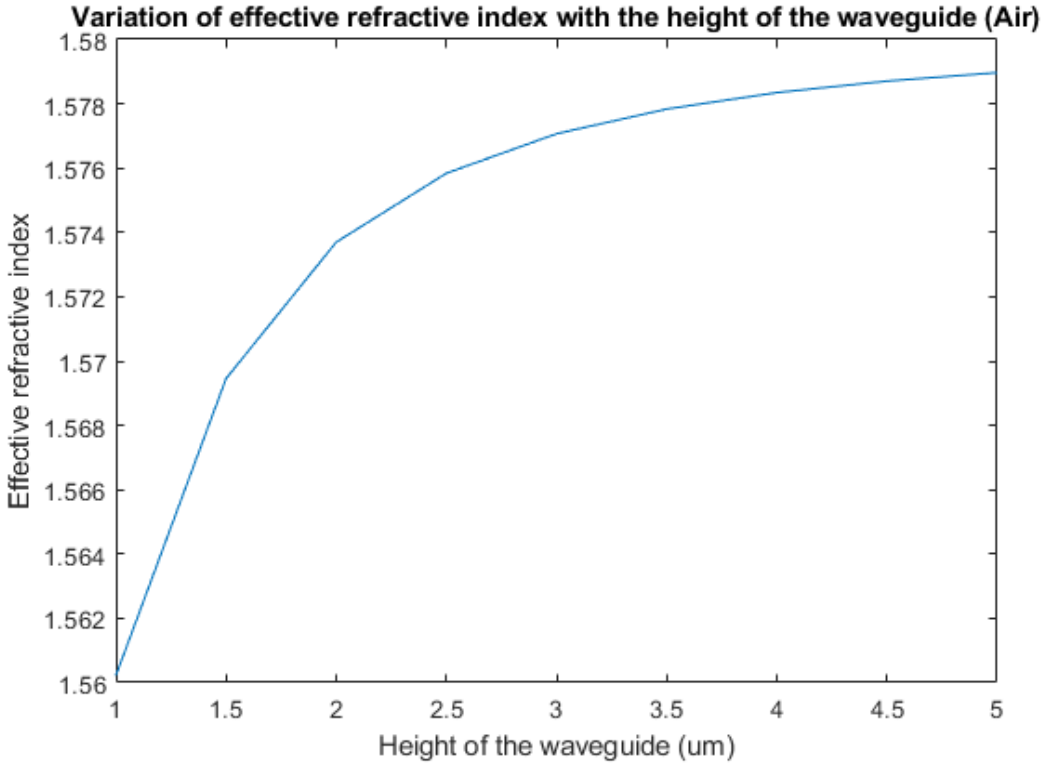

Figure 4.8: Evolution of the n_{eff} with the height of the waveguide (Air)

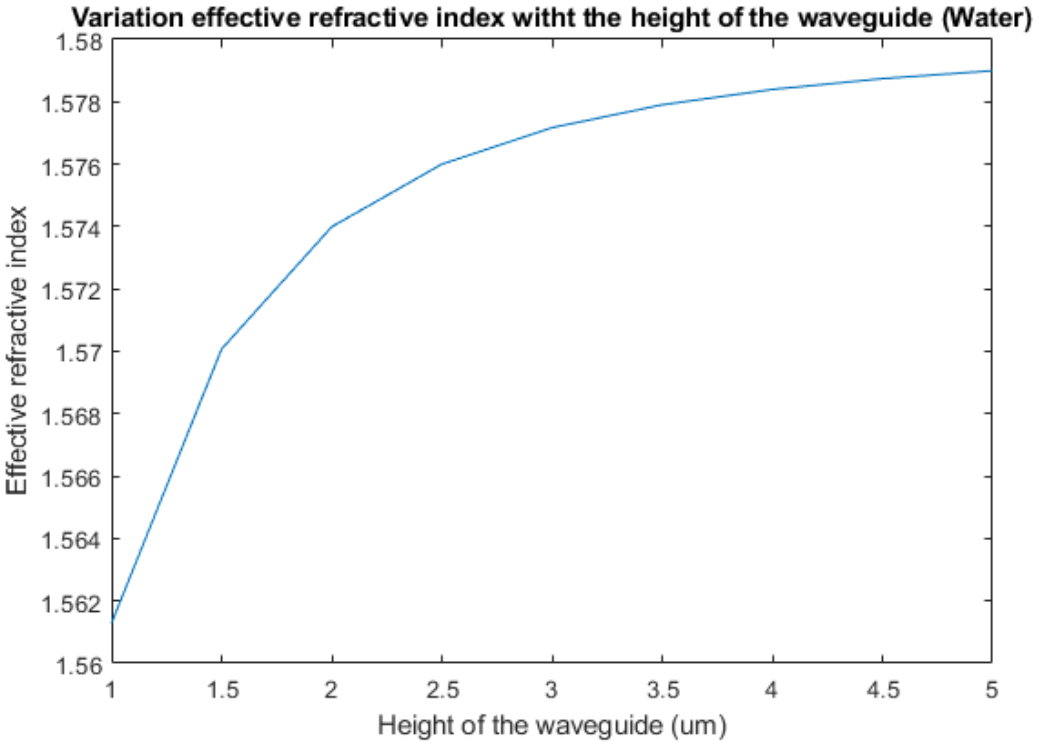

Figure 4.9: Evolution of the n_{eff} with the height of the waveguide (Water)

Through the analysis of both these graphs it is possible to observe that a height below 4 μm will lead to high variations in the n_{eff}. This could translate into a sensor that isn't robust to small defects that can come about in the fabrication process as even the slightest deviation from the expected height would make a great impact in the effective refractive index of the waveguide.

In order to avoid this problem the height chosen for the wave guide was 4.5 μm.

Using the values of the n_{eff}'s, that have been obtained, it is possible to solve the equation 4.1 which will produce a graph of the length of the sensors arms in relation to the height of the waveguide. This graph can be seen in the figure 4.10 where it is shown that the length of the arms grows exponentially with the height of the waveguide for the simulated values.

In order to have a sensor that is robust to small fabrication errors while being compact the height chosen for the waveguide was 4.5 μm as this would avoid the problem mentioned previously while only leading to an arm length of 9.3 mm.

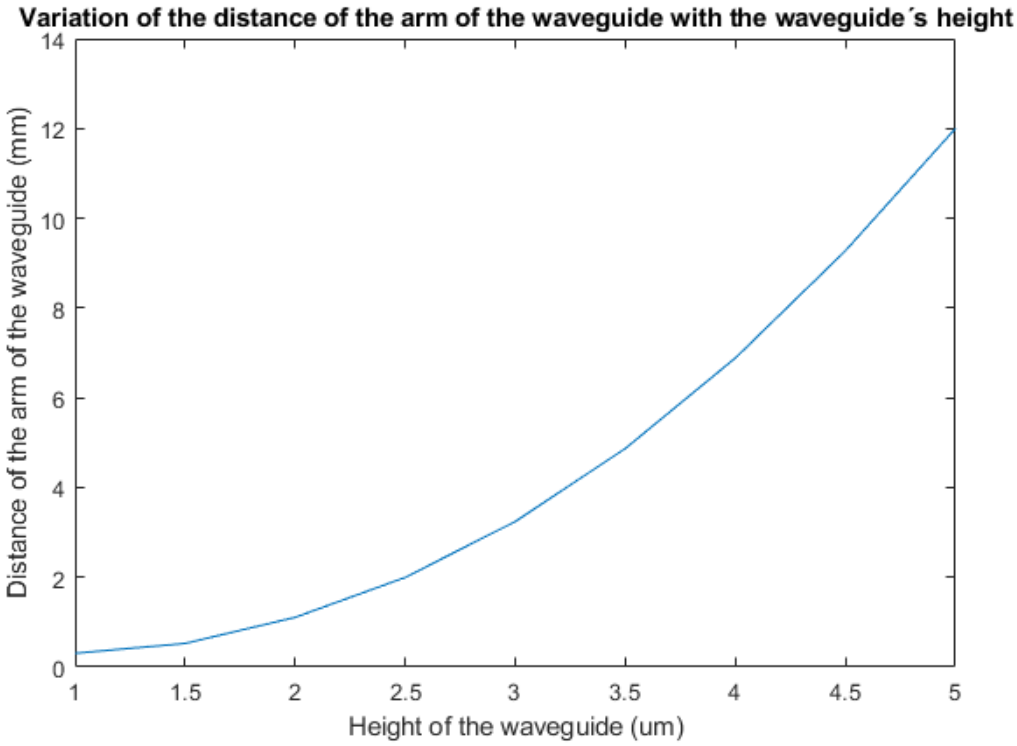

Figure 4.10: Evolution of the length of the sensor's arm with the height of the waveguide

4.3 Waveguide Bend Attenuation

Another important factor that needed to be studied was the attenuation due to the bends that are present in the sensor. As such another set of simulations were done using the Beam Propagation Method, in order to determine the attenuation that each bend would have in the output of the sensor.

The original BPM is not suited for simulating bends with high curvatures however BeamProp has an simulated bend feature which distorts the modal field shape without shifting the position of the waveguide. So as to study the effects of the bends these were added to the model using the simulated bend feature.

The simulation that was done took the model of the sensor and "added" the bends to the start of the waveguide as to observe the attenuation caused by a single bend. For this the radius of the bend was simulated between the values of 600 μm and 1200 μm. This simulation resulted in a graph with the power output after the bend for the different radius which can be seen in the figure 4.11.

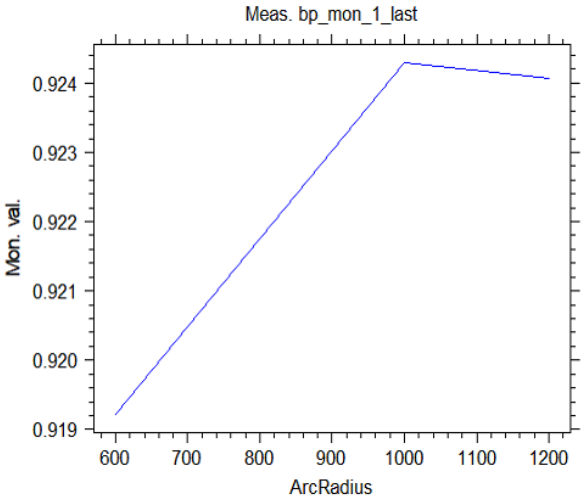

Figure 4.11: Evolution of the bend attenuation with the ArcRadius

The results of the simulation show that an arc radius in the range of 600 μm to 1200 μm would incur in an attenuation in the ranges of 0.39 dB (8.6 %) to 0.41 dB (9 %), as described by the figure 4.11, with the lowest attenuation being at an arc radius of 1000 μm.

After determining the attenuation the length of the bend was calculated as it is an important factor when designing the sensor. This was done through the equation 4.2 where the ArcFinal is $90°$ as this was the angle of the arc that was able to be drawn onto the photomask in the KiCad software.

$$L_{Bend} = 2\pi * ArcRadius * \frac{ArcFinal}{360} \tag{4.2}$$

As such the length of the bend was calculated for the simulated values of the radius which lead to the graph present in the figure 4.12.

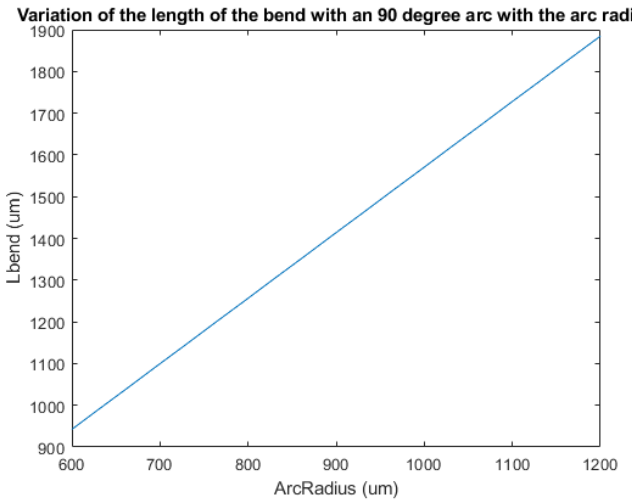

Figure 4.12: Length of the bend for the respective arc radius

Taking both results into consideration the arc radius chosen was that of 600 μm. While this radius does not translate into the lowest attenuation it

does reduce the size of the sensor, as it is shown by the length of the bend of 942.5 μm while maintaining an attenuation of 0.41 dB (9 %) as this can be considered a reasonable value.

4.4 Input Coupling

The input coupling is going to be an inevitable factor in the study of the sensor due to the fact that the light will be injected into the waveguide from a optical fiber. For this reason the study of the input coupling and the optimal distances and tilt of the fiber is a necessity. As such another series of simulations were done as to ascertain the optimal values of distance, from the fiber to the waveguide, as well as the tilt and horizontal and vertical alignment of the fiber.

Firstly it was added a launch field in the simulation environment, as this would be the equivalent of a light source (in this case a laser working on the 635 nm wavelength). The launch field, emulating the fiber, was placed at a distance of 5 μm to the waveguide as a starting point and was moved further until it reached a distance of 95 μm in order to see the intensity of the light that would enter the waveguide. This simulation produced the results shown in the figure 4.13 where it can be seen that at best the attenuation for these sets of distances would be in the 3 dB (50 %) with a massive drop off at the 15 μm where the power reaching the waveguide would be below the -10 dB (10%). This would prove to be a problem as in order to compensate this loss the power source would need to have an higher output.

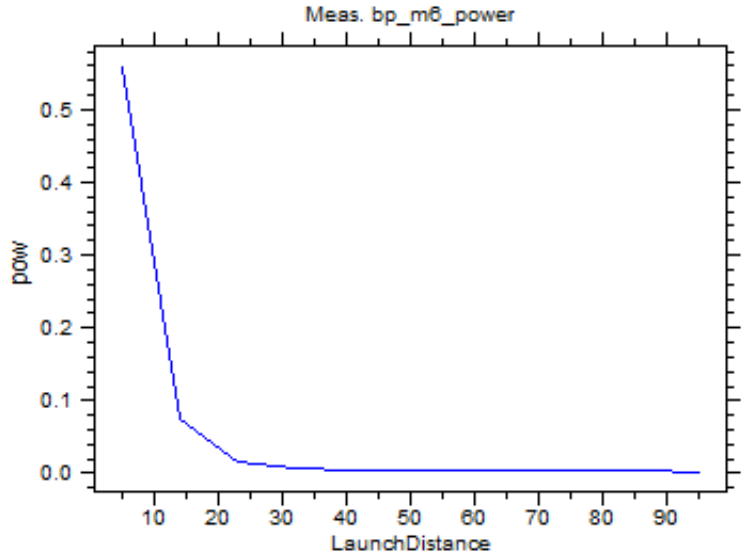

Figure 4.13: Power reaching the start of the bend in the waveguide following the input coupling from the fiber to the waveguide at a distance from 5 to 95 μm

Following the less then ideal results yielded from the first simulation a second set was done in order to find an optimal distance from the waveguide. As such the distance of the source was moved between the 1 μm to 5 μm. Through this new set of simulations it is possible to observe that for distances lower than 2.5 μm the attenuation is below the 0.457 dB (10 %) as seen in the figure 4.14. With these results the distance that was considered as optimal was the 2 μm as it would give some margin for error while maintaining an output of more than 90 % of the original power.

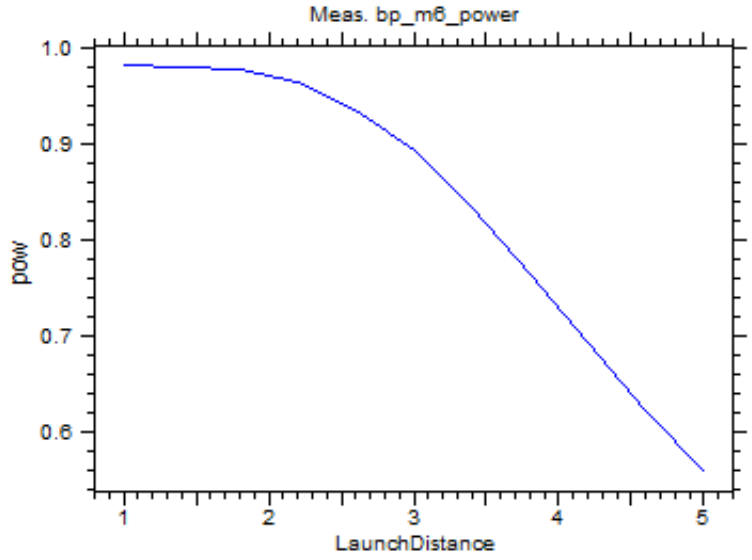

Figure 4.14: Power reaching the start of the bend in the waveguide following the input coupling from the fiber to the waveguide at a distance from 1 to 5 μm

After the previous simulations and having set an optimal distance (2 μm) another study was done in order to determine the effects that an offset in angular position would have in the input coupling. In the figure 4.15 an illustration of what the following simulations are emulating is shown.

The simulations were divided into two parts, one would determine the effects that a tilt in the azimuth (represented in the figure 4.15 as ϕ) and elevation (represented in the figure 4.15 as θ) would have in the input coupling and a second one that would determine the effects of an offset in the vertical and horizontal plane would have in the coupling.

For this effect in the first instance the azimuth ($-30° < \phi < 30°$) and the elevation ($-10° < \theta < 10°$) of the source were changed with the results shown in the figure 4.16.

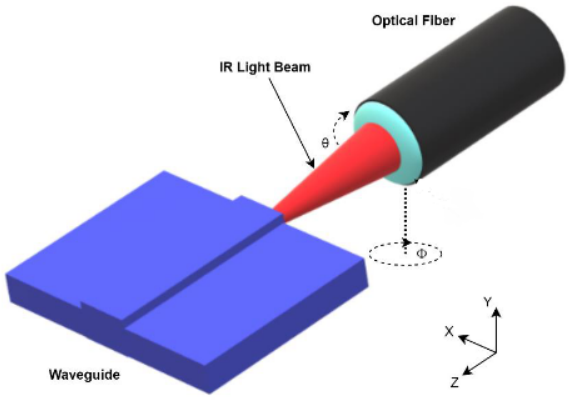

Figure 4.15: Illustration of the input coupling (adapted from[13])

Analyzing the results it is evident that a variation, either positive or negative, of $4°$ in azimuth and $5°$ in elevation leads to approximately same value in overlap of 0.7671, corresponding to an attenuation of 1.19 dB (red region in the figure 4.16) meaning that the sensor is impervious to any tilt within that range.

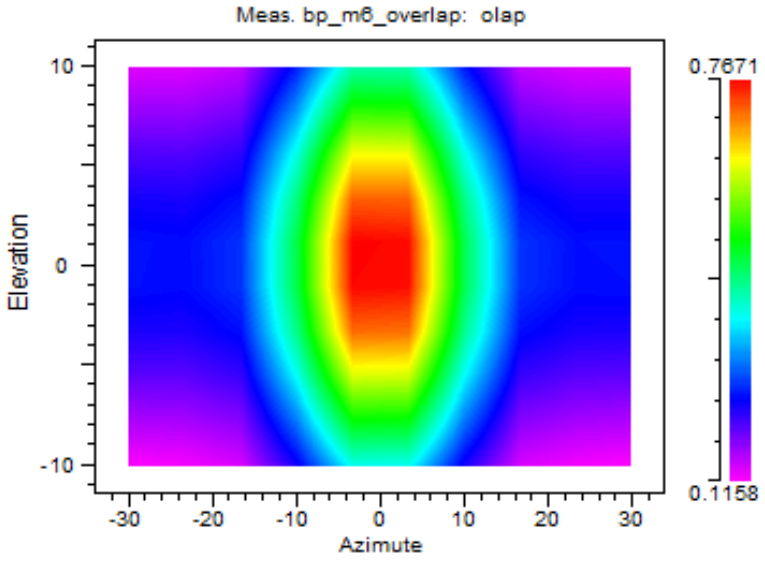

Figure 4.16: Color coded overlap at the input of the waveguide in relation to the azimuth and elevation of the source

In the second instance of simulations in order to see the effects caused by the horizontal and vertical offsets the source was shifted on both planes more specifically having an offset in the horizontal plane of $-2\ \mu$m $<$ x $< 2\ \mu$m and in the vertical plane $-2\ \mu$m $<$ y $< 2\ \mu$m. This lead to the results displayed in the figure 4.17.

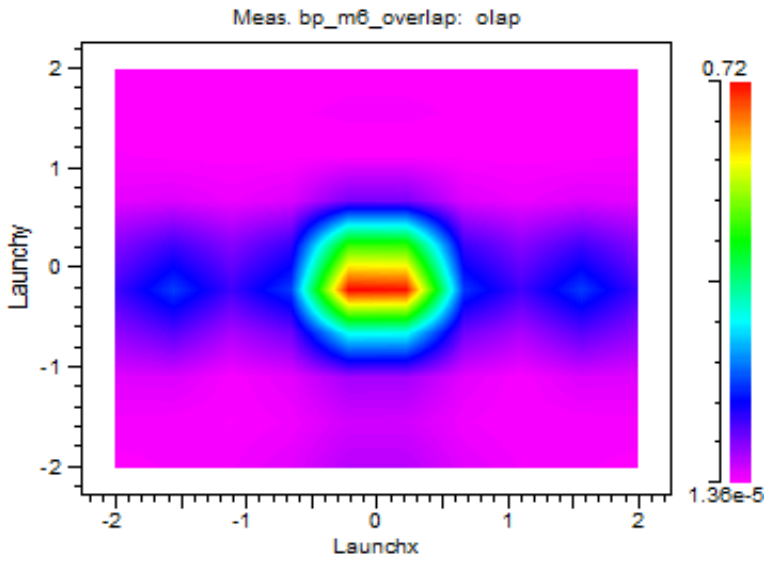

Figure 4.17: Color coded overlap at the input of the waveguide in relation to the horizontal and vertical offset of the source

In terms of alignment any shift in the 0.2 μm range in the vertical plane and 0.4 μm in the horizontal plane leads approximately to the same overlap power of 0.72, corresponding to an attenuation of 1.43 dB.

The simulations show that in order to get the best input coupling the source should be distanced from the waveguide by 2 μm while having a tilt of no more than 5° in elevation and 4° in azimuth, as well as avoiding having an offset of more than 0.2 μm in the vertical plane and 0.4 μm in the horizontal plane.

4.5 Microfluidics Study

In order to test the effects of the microfluidic system when implemented onto the sensor some tests where ran. In these simulations the sensor dimensions used were the ones calculated in the previous sections of this thesis. On this model a channel was added in order to simulate the microfluidics system as seen in the image 4.18. To achieve this model the top part of the sensor was covered by PDMS material (identified by the green color in the image) leaving a channel of air (identified by the white color on the image) between the PDMS and the waveguide.

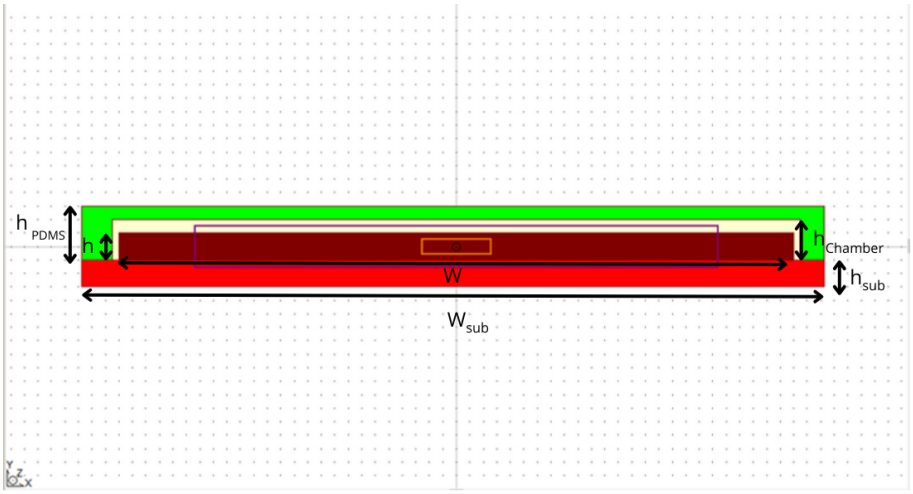

Figure 4.18: Frontal view of the sensor
Color label :Green - PDMS microfluidics chamber
Dark Red - SU-8 Waveguide
Light Red - Corning Glass Substrate

In order to begin the simulations the refractive index of the PDMS had to be defined as well as the height of the PDMS material since both of these were parameters necessary for the simulation. As for the refractive index of the PDMS it was found to be 1.4009 for the 635 nm wavelength and the height was initially assumed to be 8 μm.

The aim of the simulations was to calculate the optimal height of the channel which wouldn't cause a change in the length of the interferometers arms. As such the height of the channel was altered between 2μm and 8μm.

From the results of the simulations it was possible to calculate the length of the arms of the interferometer for the dimensions mentioned which produced the following graph 4.19.

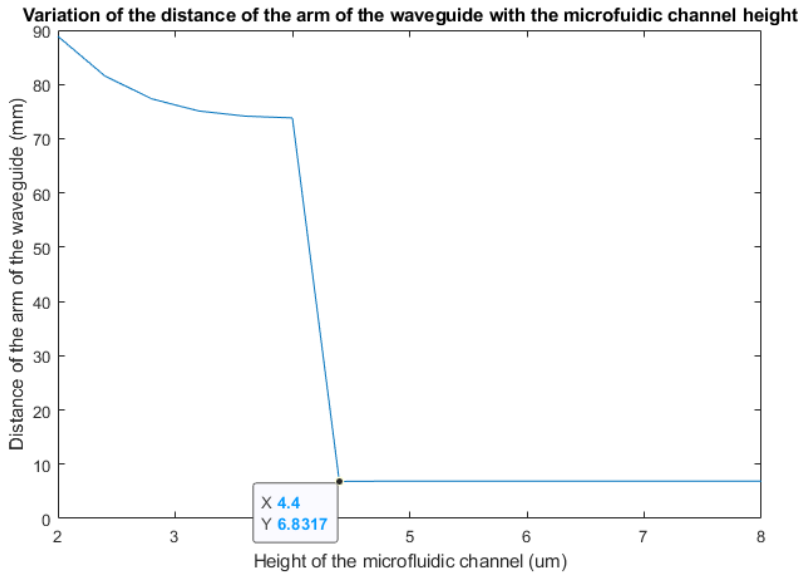

Figure 4.19: Variation of the Arm Length with the Channel height

The results show that for a channel height of more than 4.4 μm the length of the interferometer would be in the 6.8 mm range. This would mean that the introduction of a microfluidic system would shorten the length of the sensor from 9.3 mm to 6.8 mm in order to achieve the same result.

4.6 Final Photomask

As mentioned in the methods section the photomask was designed with the use of the *KiCad* software. The designed had to have in consideration the paremeters established in the simulations such as the arm length, the arc radius, as well as the limitations of the materials and methods that were available and thought of for this work.

The arms are 4 mm apart as to leave enough room for a drop of the sample to be deposited onto one arm while not contaminating the other. The other parameters that were taken into account are the arc radius of the bends which was stated to be 600 μm and an arm length of 6.8 mm as calculated in the previous section.

The final mask can be seen in the image 4.20.

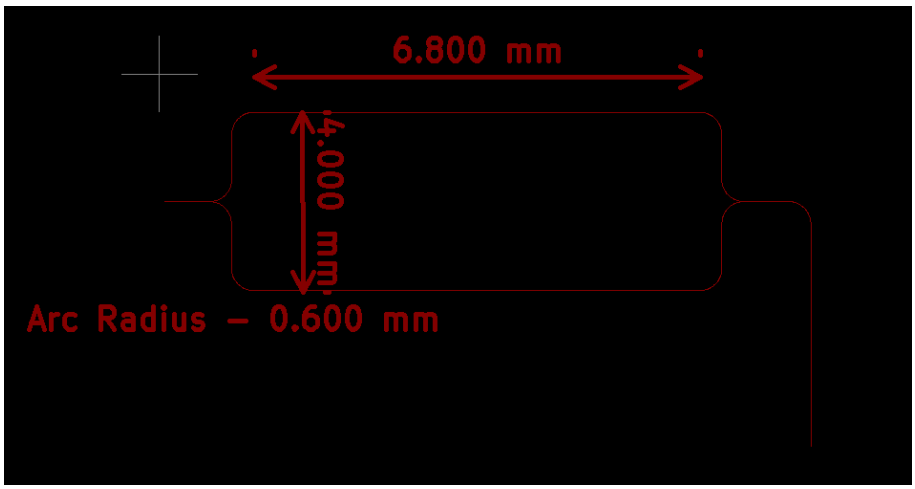

Figure 4.20: Sensors Mask

5
Conclusion and Future Work

5.1 Conclusion

This thesis had the goal of studying the feasibility of a sensor with multimicron dimensions based on a Mach-Zehnder interferometer using a negative photoresist polymer with the added feature of being adaptable for a microfluidic system. For this reason a theoretical study was done with the use of simulation tools which helped to confirm, in theory, the possibility of such device being achievable.

As stated before the work done was theoretical, even so the simulations done resulted in a concept of a sensor that could be fabricated and worked with a laser source in the 635 nm region.

The simulations done show the possibility of designing a Mach-Zehnder interferometer with the waveguide made in a negative photoresist polymer, namely the SU-8 polymer, with dimensions of 10 μm in width and 4.5 μm in height while having a substrate made of corning glass with a height of 2 μm and a width of 12 μm as this would lead to an arm length of 9.3 mm.

The work done also studied the modes propagating through the waveguide mainly the TM fundamental mode as this is the optimal mode for this sensor's application. This is due to the fact that the sensor works using an evanescent field based detection and the TM fundamental mode as a higher tendency to leak out of the waveguide, in the vertical direction, making it more sensitive to the surrounding medium (analyte).

A study on the attenuation was also conducted. Firstly the waveguide bend attenuation was evaluated. The results of these simulations show that even at the lowest simulated arc radius the bend attenuation would be at an acceptable level, as the loss in the bend would be of 0.41 dB meaning that the signal output after the bend would retain roughly 90 % of the original power. This made it so that the arc radius chosen for the sensor was of 600 μm as

this would lead to the lowest bend length of 942.5 μm while maintaining the previously mentioned level of attenuation.

There was also a focus in the input coupling since it was assumed that the laser would be injected into the waveguide through an optical fiber. This showed a good end-fire efficiency for a fiber located at a distance 2 μm from the waveguide, as the wave maintained 90% of the original power. The vertical and horizontal offset also produced an acceptable attenuation of 1.43 dB within the range of -0.2 to 0.2 μm for the vertical offset and -0.4 to 0.4 μm for an horizontal offset when referenced from the center of the waveguide. As for the tilt of the fiber any tilt in the range of -4° to 4° for the azimuth and -5° to 5° for the elevation lead to an attenuation of 1.19 dB.

This sensor was then studied to be fitted with a microfluidics system. This was done by implementing a microfluidics chamber onto the sensor. The chamber was material was considered to be PDMS and was placed on top of the waveguide completely covering it. A study was done in order to determine the height of the channel which came to be 4.4 μm. This channel would impact the length of the arm of the sensors as they would need to be shortened from 9.3 mm to 6.8 mm. As a result a photo mask was then designed in the appropriate software having all the previous values in consideration.

5.2 Future Work

Unfortunately it was not possible to realize and test the sensor. As such for future work the fabrication, test and optimization of the sensor for different analytes would be needed. Although the practical side of this work was not done it was taken into consideration as most of the work was based on the techniques that were going to be used in the fabrication process (mentioned in the Methods used in Sensor Production section of the work) as well as the materials that were to be used in the completion and the testing of the sensor.

For this reason the materials that were chosen are listed below with the reasoning for their choice being the availability in the lab.

The photomask was also designed as it can be later used for the fabrication of the sensor. The mask is also shown below

Photomask

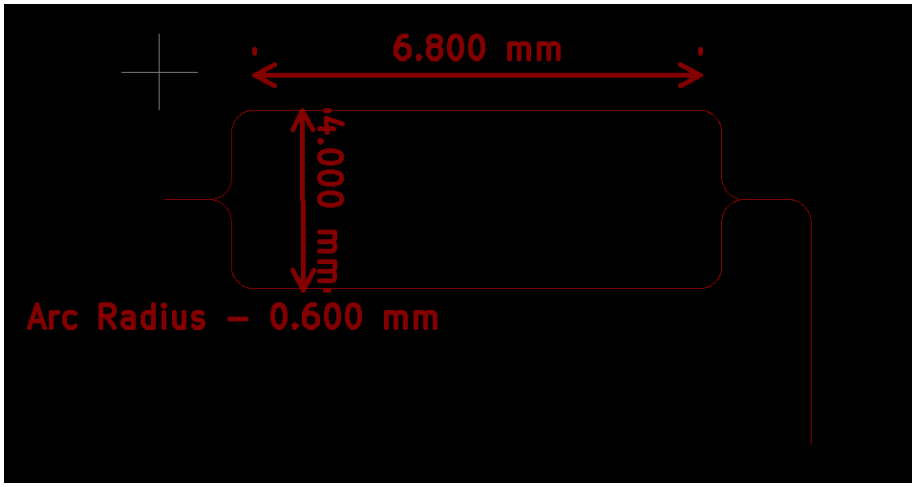

Figure 5.1: Sensors Mask to be used in the production of the sensor

Laser Source

In order to have a signal to test the sensor there has to be a source. For this purpose the laser source chosen was the K-Cube Laser Source - KLS635 (Figure 5.2). This laser source has a measure of 121 mm x 60 mm x 47 mm and operates in constant optical power mode and on a wavelength of 635 nm.

Figure 5.2: K-Cube Laser Source - KLS635 (adapted from [14])

Single Mode Fiber

A single mode fiber is at its core an optical fiber that is designed to carry a single mode of propagation.

The fiber to be used is the LP635-SF8 which is a single mode fiber designed for the wavelength of 635 nm, which is the wavelength of the laser source.

This fiber is to be used in order to get the light from he laser source onto the waveguide as exemplified in the representation 5.3

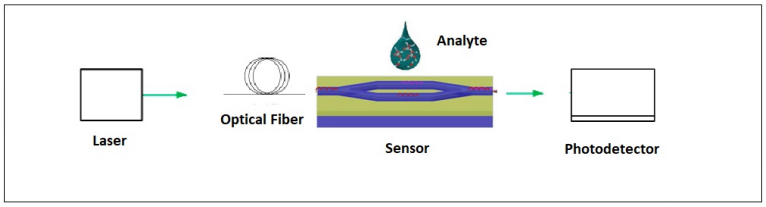

Figure 5.3: Representation of the sensing system

Fiber Polarization Controller

The FPC022 - Fiber Polarization Controller is to be used as the polarization controller. These manual polarization controllers utilize stress-induced birefringence to alter the polarization in single mode fiber that is looped around two or three independent spools to create two or three independent fractional wave plates (fiber retarders).

The retardance can be calculated through the following equation(5.1):

$$\phi(Rad) = \frac{2\pi^2 a N d^2}{\lambda D} \tag{5.1}$$

Where ϕ is the retardance, a is a constant (0.133 for this silica fiber), N is the number of loops, d is is the fiber cladding diameter, λ is the wavelength and D is the loop diameter.[32]

Polarizer

In essence a polarizer is an optical filter that blocks all light waves except the ones with a specific polarization.

The polarizer used here is a calcite polarizer which separates unpolarized light into two separate plane polarized beams as exemplified in figure 5.4. Glan Laser polarizers are designed for demanding applications requiring extreme polarization purity and high resistance to laser damage. These polarizers are air-spaced, select-grade calcite prism pairs with the prism interface angles optimized for minimum insertion loss. [15]

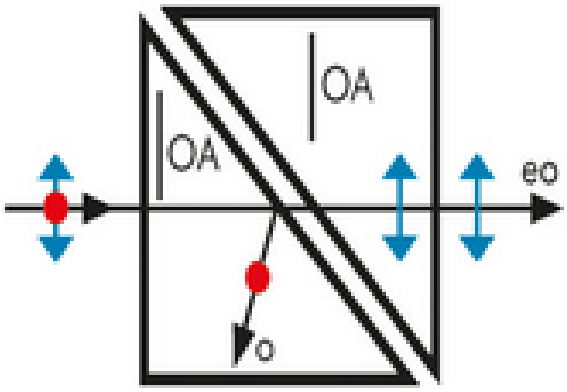

Figure 5.4: Representation of a Glan-laser Polarizer (adapted from [15])

The Glan-Laser Calcite Polarizer was the polarizer chosen to be used in this work as it is designed for high-energy laser light, high extinction ratio for output beam (100 000:1) and an AR-coating for 350-700 nm wavelength range.

Photodiode

As the the name suggest the photodiode is a diode that is sensible to photon radiation, this can be visible, infra-red or ultraviolet, X-rays and gamma rays. In laymans terms the photodiode produces an electrical current as it absorbs photons. This is normally used for detection and measurement applications.

The S150C - Compact Fiber Photodiode Power Sensor is designed for fiber based applications in the VIS and NIR wavelength range without having a disturbing cable between sensor head and power meter console. The head is spectrally calibrated over the whole wavelength operating range and detects light from nano watts up to 5 mW.[33]

Power Meter

The power meter is one of the most useful and simple instruments to measure electrical power.

The Power and Energy Meter Interfaces with External Readout from *THORLABS* was chosen for the flexibility and adaptability it provides for specific measurements since it has a selectable bandwidth of 20 hz to 100 kHz with the lower bandwidth providing better accuracy.

Bibliography

[1] C. Song and S. H. Tan, “A perspective on the rise of optofluidics and the future,” *Micromachines*, vol. 8, 2017.

[2] N. Bakhla, P. Laxmi, and P. Gangopadhyay, “Su-8 polymer as an optical waveguide for integrated optics su-8 polymer as an optical waveguide for integrated optics view project avalanche photo-detectors & single photon counting view project priya lakshmi manipal academy of higher education journal of electronic design technology su-8 polymer as an optical waveguide for integrated optics,” 2019. [Online]. Available: https://www.researchgate.net/publication/348340089

[3] K. A. Materials, “Technical data sheet su-8 2000, Aug. 2020.”

[4] “Optical components for matrix processing — by michael gould — lightmatter — medium.” [Online]. Available: https://medium.com/lightmatter/optical-components-for-matrix-processing-73687cdd7aa6

[5] “Spin coating - solid state chemistry.” [Online]. Available: https://wiki.aalto.fi/display/SSC/Spin+coating

[6] J. P. Singh, R. Bhardwaj, A. Sharma, B. Kaur, S. O. Won, S. Gautam, and K. H. Chae, “Fabrication of magnetic tunnel junctions,” *Advanced Applications in Manufacturing Engineering*, pp. 53–77, 1 2019.

[7] A. Buzzin, R. Asquini, D. Caputo, and G. de Cesare, “On-glass integrated su-8 waveguide and amorphous silicon photosensor for on-chip detection of biomolecules: Feasibility study on hemoglobin sensing,” *Sensors (Switzerland)*, vol. 21, pp. 1–14, 1 2021.

[8] N. Pelletier, B. Bêche, N. Tahani, J. Zyss, L. Camberlein, and E. Gaviot, “Su-8 waveguiding interferometric micro-sensor for gage pressure measurement,” *Sensors and Actuators, A: Physical*, vol. 135, pp. 179–184, 3 2007.

[9] S. Psoma, M. Kusko, D. Esinenco, S. D. Psoma, M. Kusko, A. Schneider, and R. Muller, “Su-8 micro-biosensor based on

mach-zehnder interferometer," pp. 295–299, 2005. [Online]. Available: https://www.researchgate.net/publication/267860436

[10] D. Martens and P. Bienstman, "Study on the limit of detection in mzi-based biosensor systems," *Scientific Reports*, vol. 9, 12 2019.

[11] "Direct writing - lnf wiki." [Online]. Available: https://lnf-wiki.eecs.umich.edu/wiki/Direct_writing

[12] D. Yuan, Y. Dong, Y. Liu, and T. Li, "Mach-zehnder interferometer biochemical sensor based on silicon-on-insulator rib waveguide with large cross section," *Sensors (Switzerland)*, vol. 15, pp. 21 500–21 517, 8 2015.

[13] D. Almeida, J. Costa, A. Fantoni, and M. Vieira, "Multi-micron dimensioning of amorphous silicon rib waveguides." SPIE-Intl Soc Optical Eng, 3 2022, p. 18.

[14] THORLABS, "Kls635 kls1550 k-cube laser source apt user guide original instructions kls series k-cube laser source, Mar. 2018."

[15] "Calcite polarizers selection guide: Types, features, applications — globalspec." [Online]. Available: https://www.globalspec.com/learnmore/optics_optical_components/optical_components/calcite_polarizers

[16] J. Wu and M. Gu, "Microfluidic sensing: state of the art fabrication and detection techniques," *Journal of Biomedical Optics*, vol. 16, p. 080901, 2011.

[17] S. H. Cho, J. Godin, C. H. Chen, F. S. Tsai, and Y.-H. Lo, "Microfluidic photonic integrated circuits," vol. 7135. SPIE, 11 2008, p. 71350M.

[18] I.-C. Liu, P.-C. Chen, L.-K. Chau, and G.-E. Chang, "Optofluidic refractive-index sensors employing bent waveguide structures for low-cost, rapid chemical and biomedical sensing," *Optics Express*, vol. 26, p. 273, 1 2018.

[19] J. C. Ramirez, J. N. Schianti, M. G. Almeida, A. Pavani, R. R. Panepucci, H. E. Hernandez-Figueroa, and L. H. Gabrielli, "Low-loss modified su-8 waveguides by direct laser writing at 405 nm," *Optical Materials Express*, vol. 7, p. 2651, 7 2017.

[20] C. Garcia, A. Schomacker, I. Klarholz, C. Harms, and W. Lang, "Fabrication of microfluidic devices using su-8 for detection and analysis of viruses."

[21] S. Mirzanejhad, A. Ghadi, and M. E. Daraei, "Numerical study of nanoscale biosensor based on surface plasmon polariton propagation in mach-zehnder interferometer structure," *Physica B: Condensed Matter*, vol. 557, pp. 141–146, 3 2019.

[22] T. Schubert, N. Haase, H. Ktick, and R. Gottfried-Gottfried, “Elsevier sensors and actuators A 60 (1997) 108-112 refractive-index measurements using an integrated mach-zehnder interferormeter,” 1997.

[23] M. Shwetha, M. Kumar, and K. Narayan, “Modeling and simulation of opto-fluidic based mach-zehnder interferometer for biosensing application.” Institute of Electrical and Electronics Engineers Inc., 1 2017.

[24] C. Acikgoz, M. A. Hempenius, J. Huskens, and G. J. Vancso, “Polymers in conventional and alternative lithography for the fabrication of nanostructures,” pp. 2033–2052, 2011.

[25] S. I. Najafi, M. N. Armenise, S. of Photo-Optical Instrumentation Engineers., U. S. D. A. R. P. Agency., and S. D. Library., *Functional photonic and fiber devices : 30 January-1 February 1996, San Jose, California*. SPIE, 1996.

[26] D. E. McCoy, A. V. Shneidman, A. L. Davis, and J. Aizenberg, “Finite-difference time-domain (fdtd) optical simulations: A primer for the life sciences and bio-inspired engineering,” 12 2021.

[27] Y. Tsuji, M. Koshiba, and T. Shiraishi, “Finite element beam propagation method for three-dimensional optical waveguide structures,” 1997.

[28] Y. Chung, “Papers an assessment of finite difference beam propagation method.”

[29] F. Barnes and S. R. P. Pavani, “Optical waveguide analysis using beam propagation method,” *Term Paper for'Introduction to Optoelectronics'*, 2006.

[30] M. Koshiba, Y. Tsuji, and M. Hikari, “Time-domain beam propagation method and its application to photonic crystal circuits,” 2000.

[31] I. Andonegui, A. J. Garcia-Adeva, J. J. Joannopoulos, R. D. Meade, and J. N. Winn, “The finite element method applied to the study of two-dimensional photonic crystals and resonant cavities references and links,” 2013. [Online]. Available: http://www.cise.

[32] THORLABS, “Manual fiber polarization controllers user guide, Mar. 2020.”

[33] THORLABS, “s150c-specsheet, Feb. 2009.”